# Decision-Feedback Equalization of Pulse-Position Modulation on Measured Nondirected Indoor Infrared Channels

Malik D. Audeh, *Member, IEEE*, Joseph M. Kahn, *Member, IEEE*, and John R. Barry, *Member, IEEE*

***Abstract*— We examine the performance of two decision-feedback equalizers (DFE's) for pulse-position modulation (PPM) on measured nondirected indoor infrared channels with intersymbol interference. PPM offers high average-power efficiency, but on ISI channels, unequalized PPM suffers severe performance penalties. We have previously examined the performance of the maximum-likelihood sequence detector (MLSD), and found that it yields significant improvements. However, the MLSD often requires such large complexity and delay that it may be impractical. We investigate suboptimal, reduced-complexity equalization techniques for PPM, providing a performance analysis of zero-forcing chip-rate and symbol-rate DFE's. Our results show that a symbol-rate DFE provides performance that closely approaches that of the optimal MLSD.**

***Index Terms*—Amplitude shift keying, decision feedback equalizers, demodulation, maximum-likelihood detection, optical communication, optical propagation, pulse position modulation.**

## I. Introduction

NONDIRECTED infrared (IR) radiation [1]–[7] has been shown to be a viable alternative to radio for wireless indoor communication. Many applications of nondirected IR links require high average-power efficiency to minimize ocular hazards and transmitter power consumption. Earlier work has shown $L$-pulse-position modulation ($L$-PPM) is an effective modulation technique due to its high average-power efficiency, which increases with increasing $L$ [3], [8]. However, in high-speed (>10 Mb/s) indoor IR systems, we must consider the effects of intersymbol interference (ISI), resulting from reflections off walls, floors, and room objects [5]. Because of its poor bandwidth efficiency, PPM is more severely affected by ISI than simple on–off keying (OOK).

Prati and Gagliardi [9] have investigated linear equalization for photon-counting channels. Recent work on indoor IR communications has quantified the effects of ISI on unequalized PPM systems, and the improvement obtained by using the maximum-likelihood sequence detector (MLSD) [8]. Since the complexity and delay of the MLSD may be prohibitive in many applications, three decision-feedback equalizers (DFE's) for PPM have been proposed: a symbol-rate DFE, a chip-rate DFE, and a correcting-chip-rate DFE [10]. For pulse-amplitude modulation (PAM) equalizers, the BER can be computed directly through formation of the folded spectrum and computation of the mean-squared error (MSE) [11]. However, for PPM, the MSE does not uniquely determine the BER [10]. Therefore, in this letter we develop tight bounds for the BER of the symbol-rate and chip-rate ZF-DFE's.[1]

Paper approved by J. J. O'Reilly, the Editor for Optical Communication of the IEEE Communications Society. Manuscript received August 15, 1996; revised April 15, 1998 and July 15, 1998. This work was presented in part at ICC '96, Dallas, TX, June 1996. This work was supported by National Science Foundation under Grant ECS-9408957 and under Grant NCR-9308968, by Hewlett-Packard Company, and by the University of California MICRO Program.

M. D. Audeh is with Hybrid Networks, Inc., San Jose, CA 95120 USA (e-mail: audeh@hybrid.com).

J. M. Kahn is with the Department of Electrical Engineering and Computer Sciences, University of California at Berkeley, Berkeley, CA 94720 USA.

J. R. Barry is with the Department of Electrical and Computer Engineering, Georgia Institute of Technology, Atlanta, GA 30332 USA.

Publisher Item Identifier S 0090-6778(99)03317-6.

## II. Channel and Noise Models

Our channel model [5] with intensity modulation and direct detection (IM/DD) can be summarized by $Z(t) = RX(t) \otimes h(t) + N(t)$, where the symbol $\otimes$ represents convolution. In IM, the transmitted signal $X(t)$ is an instantaneous optical power. $Z(t)$ represents the received photocurrent, while $R$ represents the photodetector responsivity. The channel is described by $h(t) \leftrightarrow H(f)$, which are fixed for a given position of the transmitter, receiver, and intervening reflectors. The additive noise $N(t)$ is modeled as white and Gaussian, and independent of the received signal. Our treatment of the noise as Gaussian and signal-independent simplifies calculation of the error probability without any significant loss of accuracy. The channel optical path loss is given by $H(0) = \int_{-\infty}^{\infty} h(t)\, dt$, and the received optical power is $P = H(0)P_t$, where $P_t$ is the transmitted power. We define the electrical SNR to be SNR $= R^2P^2/(R_bN_0)$, where $R_b$ represents system bit rate and $N_0$ represents the (two-sided) power spectral density of the white Gaussian noise. We note that a 1-dB change of optical power corresponds to a 2-dB change of electrical SNR.

## III. Chip-Rate Zero-Forcing DFE

Fig. 1(a) displays the block diagram of a discrete-time $L$-PPM system with a chip-rate ZF-DFE. Independent, identically distributed (i.i.d.) input bits $a_j$ enter a block coder of rate $(\log L)/L$, which produces length-$L$ symbol vectors having one unit chip value and $L-1$ zero chip values. The chip sequence $b_k$ is scaled by the peak received photocurrent $LPR$, and passed through the causal, minimum-phase discrete-equivalent channel impulse response $h_k$ representing the combination of transmitter filter, multipath channel, and whitened-matched filter (WMF) [12]. We assume $h_k$ is normalized such that $\Sigma_k\, h_k = 1$. The noise samples $n_k$ are white and Gaussian with variance $N_0$. The chip-rate ZF-DFE employs two decision

[1] Simulations have shown that at low BER's on typical measured channels, the performance of the correcting chip-rate DFE is indistinguishable from that of the chip-rate DFE, and that the performance of zero-forcing chip- and symbol-rate DFE's is indistinguishable from that of their minimum-MSE counterparts.

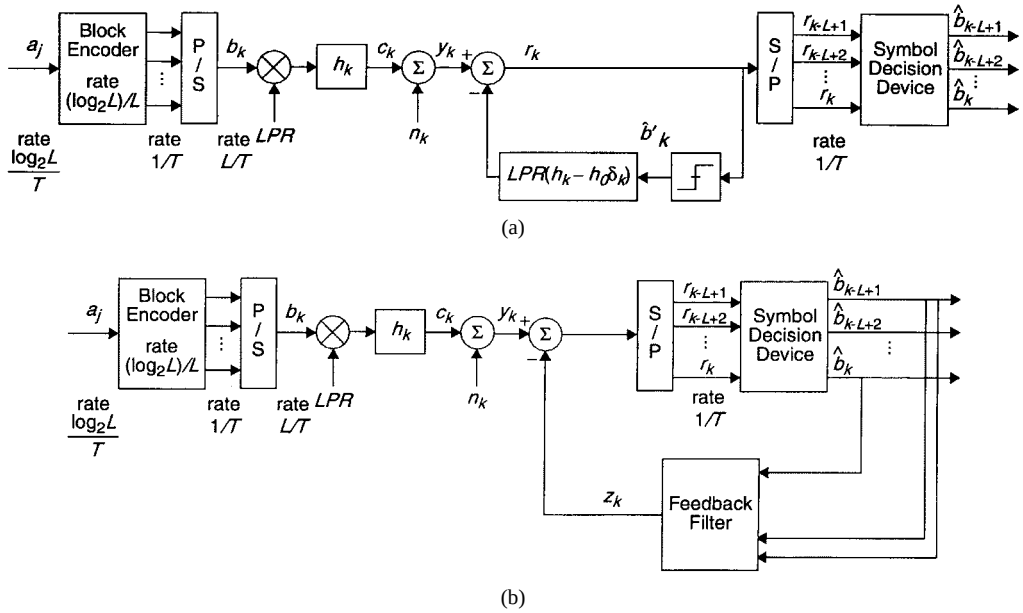


Fig. 1. $L$-PPM transmission over a multipath channel, followed by: (a) chip-rate zero-forcing decision-feedback equalizer or (b) symbol-rate zero-forcing decision-feedback equalizer. The blocks "P/S" and "S/P" represent parallel-to-serial and serial-to-parallel convertors, respectively.

devices. The first decision device, in the feedback loop of Fig. 1(a), makes chip-by-chip decisions $\hat{b}'_k$, where $\hat{b}'_k = 1$ if $r_k > \lambda$ and zero otherwise. These chip-by-chip decisions are fed back through a reverse filter $LPR(h_k - h_0\delta_k)$ containing the strictly causal portion of $h_k$. The second decision device makes symbol-by-symbol decisions, based on which is the largest of the $L$ sample values $r_{k-L+1}, \cdots, r_k$, independent of the chip-by-chip decision device.

In analyzing the error probability, we let $b = [b_0 \cdots b_{L-1}]$ denote the transmitted PPM codeword. X denotes the event that all previous chip decisions and symbol decisions from prior PPM codewords are correct, a standard assumption in DFE analyses [13]. Assuming $e_j$ is the $L \times 1$ vector of all zeros except for a single one at position $j \in \{0, \cdots, L-1\}$, we find:

$$
\begin{aligned}
&P[\text{symbol error}|\text{X}] \\
&= \frac{1}{L}\sum_{l=0}^{L-1}\{P[\text{error}|\text{X}, b = e_l]\} \\
&= \frac{1}{L}\sum_{l=0}^{L-1}\Big\{P[\text{error}|\text{X}, \hat{b}' = b, b = e_l]P[\hat{b}' = b|\text{X}, b = e_l] \\
&\quad + \sum_{j=0}^{l-1} P[\text{error}|\text{X}, \hat{b}' - b = e_j, b = e_l] \\
&\quad \cdot P[\hat{b}' - b = e_j|\text{X}, b = e_l] + P[\text{error}|\text{X}, \hat{b}' = 0, b = e_l] \\
&\quad \cdot P[\hat{b}' = 0|\text{X}, b = e_l] + \sum_{j=l+1}^{L-1} P[\text{error}|\text{X}, \hat{b}' - b = e_j, b = e_l] \\
&\quad \cdot P[\hat{b}' - b = e_j|\text{X}, b = e_l] \\
&\quad + P[\text{error}|\text{X}, w_H(\hat{b}' - b) \geq 2, b = e_l] \\
&\quad \cdot P[w_H(\hat{b}' - b) \geq 2|b = e_l]\Big\}. \qquad (1)
\end{aligned}
$$

The symbol $w_H$ refers to the Hamming weight. A more compact expression for (1) is

$$
\begin{aligned}
&P[\text{symbol error}|\text{X}] \\
&\quad = \frac{1}{L}\sum_{l=0}^{L-1}\Bigg\{P_0\pi_0 + \sum_{j=0}^{l-1} P_{1,j}\pi_{1,j} + P_2\pi_2 \\
&\qquad + \sum_{j=l+1}^{L-1} P_{3,j}\pi_{3,j} + P_4\pi_4\Bigg\}. \qquad (2)
\end{aligned}
$$

The notation in (2) is defined by drawing a one-to-one correspondence between the terms in (2) and those in (1). We note that $P_0 = 0$ since a symbol error can occur only if a chip error occurs. To simplify subsequent expressions, we let $\eta_k = LPRh_k/\sqrt{N_0}$ represent the normalized impulse response. The normalized threshold of the chip-rate slicer is set to the minimax value of $\lambda = \eta_0/2$, which maximizes $\pi_0$, the probability of all chips being detected correctly. In what follows, we give exact expressions for the terms in (2), except for $P_4$, which is intractable. Consequently, we bound the error probability.

The symbol-decision error described by $P_{1,j}$ in (2) occurs when a chip (represented by $j$) prior to the transmitted chip (represented by $l$) is detected above the threshold, and therefore, in error. As a result, we know that one noise sample (we will denote it $z_1$) is above $\lambda$, and is thus described by a truncated Gaussian distribution. Following [8], we find below the probability of a symbol error $P_{1,j}$

$$
\begin{aligned}
P_{1,j} = 1 - E\Bigg[&(1 - Q_{1,0}(z_1 + \eta_0 - \eta_{l-j}))^j \\
&\times (1 - Q_{1,j}(z_1 + \eta_0 - \eta_{l-j})) \\
&\times \prod_{i=j+1\neq l}^{L-1} (1 - Q(z_1 + \eta_0 - \eta_{l-j} + \eta_{i-j}))\Bigg]. \qquad (3)
\end{aligned}
$$

Here $Q_{1,i}(x) = \max\{[Q(x) - Q(\lambda + \eta_{i-j})]/[1 - Q(\lambda + \eta_{i-j})], 0\}, i \neq j$ and $Q_{1,j}(x) = \min\{Q(x)/Q(\lambda), 1\}$. Since $z_1$ is a truncated Gaussian random variable, (3) is not analytically tractable, so we resort to numerical integration to evaluate (3) for actual channels. The probability of the event whereby one chip error prior to the transmitted chip occurs is given by:

$$\pi_{1,j} = (1 - Q(\lambda))^j Q(\lambda) \prod_{i=j+1}^{l-1} (1 - Q(\eta_{i-j} + \lambda)) \times Q(\eta_{l-j} - \eta_0 + \lambda) \prod_{i=l+1}^{L-1} (1 - Q(\eta_{i-j} - \eta_{i-l} + \lambda)) \tag{4}$$

The symbol-decision error described by $P_2$ in (2) occurs when the transmitted chip is detected in error. More specifically, this means that none of the $L$ chips is greater than $\lambda$. We let $z_2$ represent the one noise sample (in position $l$) that is less than the threshold. In this case

$$P_2 = 1 - E\left[(1 - Q_{2,0}(z_2 + \eta_0))^l \times \prod_{i=l+1}^{L-1} (1 - Q_{2,l}(z_2 + \eta_0 - \eta_{i-l}))\right]. \tag{5}$$

$Q_{2,i}$ is given by an expression analogous to that of $Q_{1,i}$, with $\eta_{i-j}$ replaced by $\eta_{i-l}$. The probability of the event where no chips are above the threshold is given by $\pi_2$:

$$\pi_2 = (1 - Q(\lambda))^l \prod_{i=0}^{L-1-l} (Q(\eta_i - \lambda)). \tag{6}$$

The symbol-decision error described by $P_{3,j}$ in (2) occurs when the a chip (represented by $j$) following the transmitted chip is detected in error, specifically, it is greater than $\lambda$. We let $z_3$ represent that noise sample that is greater than the threshold and find:

$$P_{3,l} = 1 - E\left[(1 - Q_{1,0}(z_3 + \eta_0))^j \times \prod_{i=j+1}^{L-1} (1 - Q_{1,i}(z_3 + \eta_0 + \eta_{i-j}))\right]. \tag{7}$$

As stated earlier, the computation of $P_4$, which represents events where more than one chip is detected incorrectly, is intractable. We can compute a lower bound for $P[\text{error}|\text{X}]$ by letting $P_4 = 0$. We can calculate an upper bound for $P[\text{error}|\text{X}]$ by letting $P_4 = (L-1)/L$, i.e., a random selection among $L$ choices. For this upper bound, we must then compute $\pi_4 = 1 - (\pi_0 + \pi_1 + \pi_2 + \pi_3)$. The factor $\pi_0$ represents the probability that all chips in the symbol are detected properly and is given simply by $1 - LQ(\lambda)$.

Finally, to obtain the probability of bit error [11], we multiply the symbol-error probability given by (1) or (2) by the factor $L/2(L-1)$.

## IV. Symbol-Rate Zero-Forcing DFE

The block diagram for the system with a symbol-rate ZF-DFE is shown in Fig. 1(b). The symbol-rate ZF-DFE feeds back *symbol* decisions, not intermediate chip decisions [3]. The feedback filter differs from the chip-rate DFE in that it feeds back appropriate values to cancel all postcursor intersymbol interference, but does not cancel intrasymbol interference. We let $N_s$ represent the largest number of symbols that can be spanned by $h_k$. At each time $k = JL-1$, where $J$ is an integer, a symbol decision is made; the resultant vector $\hat{b}_{k-L+1}, \cdots, \hat{b}_k$ of length $L$ is input to the feedback filter and produces output $z_k$ given by:

$$z_k = LPR \sum_{i=1}^{N_i - 1} ((\hat{b}_{k-iL+l_i})\delta_k) \otimes (h_{k+iL-l_i} u_k) \tag{8}$$

where $l_i \in \{0, \cdots, L-1\}$, $i = 1, \cdots, N_s - 1$ represent previously detected symbols. A minimum-Euclidean-distance detector operates on the received samples $r_{k-L+1}, \cdots, r_k$. The symbol decision device chooses the detected symbol to minimize $\Sigma_{k=0}^{L-1} |r_k - LPR(\hat{b}_k \otimes h_k)|^2$ over the $L$ possible choices of $\hat{b}_k$.

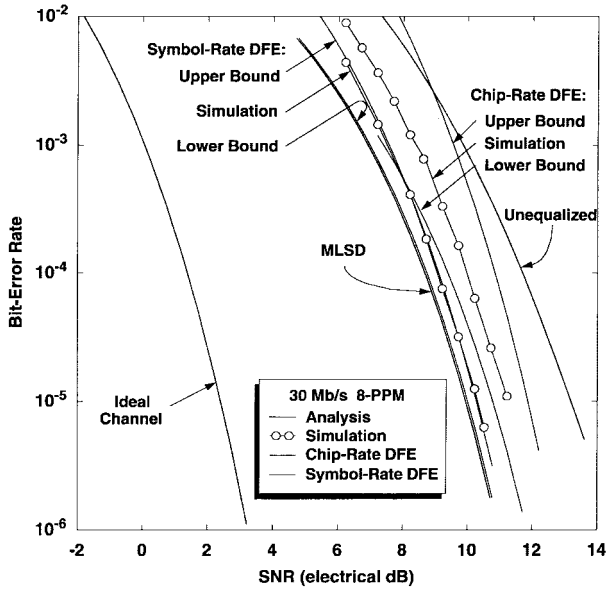


Fig. 2. BER versus electrical SNR for an 8-PPM system operating at 30 Mb/s over a typical multipath channel, comparing results of analysis and simulation for chip-rate and symbol-rate zero-forcing DFE's.

Our error-probability analysis relies upon the standard assumption that all previous symbols have been detected correctly, and that symbol-to-symbol error propagation can be ignored. To compute the BER, we find the BER conditioned on the transmission of each of the $L$ possible symbols, and then average over these:

$$P[\text{bit error}] = \frac{1}{L} \sum_{l=1}^{L} P[\text{bit error}|b = c_l] \tag{9}$$

We will compute lower and upper (union) bounds on the conditional probabilities in (9). Define the normalized Euclidean distance between transmitted symbol $l$ and another symbol $n$ as $d_{nl}^2 = \Sigma_{k=0}^{L-1} |\eta_k \otimes (b_k^{(n)} - b_k^{(l)})|^2$, where $b_k^{(n)}$ corresponds to the vector of values $b_k$ for symbol $n$ and we recall that $\eta_k = LPRh_k/\sqrt{N_0}$. To obtain lower bounds on the conditional probabilities in (9), we find the minimum Euclidean distance

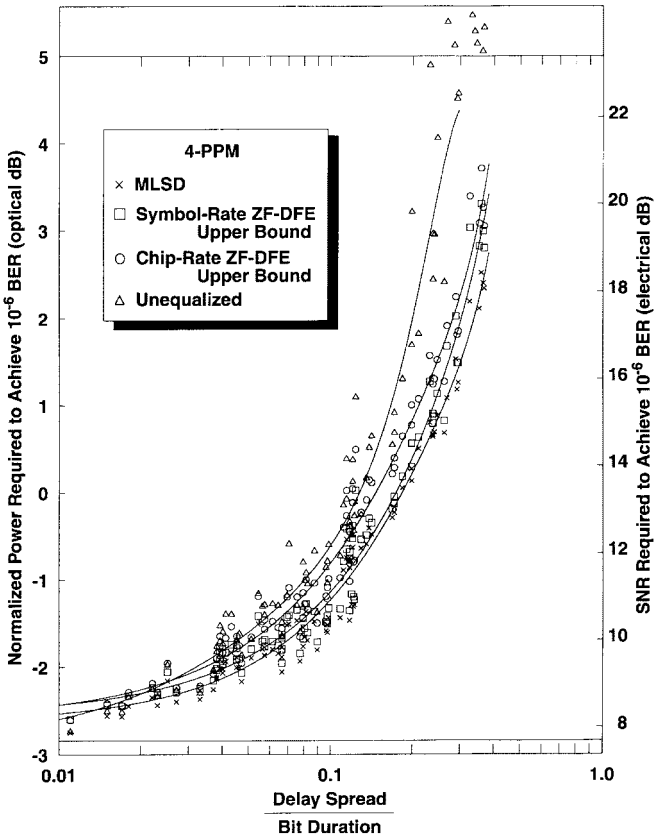


Fig. 3. Normalized average optical power (left axis) and electrical SNR (right axis) required to achieve $10^{-6}$ BER versus rms delay spread divided by bit duration for 4-PPM systems with four different detection schemes. Power requirements are normalized such that 0 dB represents the average optical power required to acheive $10^{-6}$ BER on an ideal channel using OOK. Points lying in the shaded region have normalized power requirements greater than 5 dB. The dashed line represents performance over an ideal channel. The solid lines represent fourth-order least-squares polynomial fits to the data for each modulation scheme.

for transmitted symbol $l$, i.e., $d^2_{\min,l} = \min_{n\in\{1,\cdots,L\},n\neq l} d^2_{nl}$. The lower bound is

$$P[\text{bit error}|b=e_l] > \frac{L/2}{L-1} Q\left(\frac{d_{\min,l}}{2}\right). \tag{10}$$

Upper bounds on these conditional probabilities are found by considering all possible erroneous symbols for each transmitted symbol $l$:

$$P[\text{bit error}|b=e_l] < \frac{L/2}{L-1} \sum_{\substack{n\in\{1,\cdots L\}\\ n\neq l}} Q\left(\frac{d_{nl}}{2}\right). \tag{11}$$

## V. Performance on Measured Channels

In this section, we quantify the performance of the chip- and symbol-rate ZF-DFE's on a collection of 46 experimentally measured channels [5]. To verify the accuracy of the theory given in Sections III and IV, we performed Monte-Carlo simulations of the performance of these DFE's on a typical multipath channel [5], using 8-PPM at a bit rate of 30 Mb/s. We assume a rectangular-pulse transmitter filter of duration equal to one chip. The results are shown in Fig. 2. The analytical lower bound for the symbol-rate ZF-DFE performance is nearly equivalent to the MLSD performance, but the results of our simulation approach the calculated symbol-rate ZF-DFE upper bound as the SNR increases. For the chip-rate ZF-DFE, we observe that at low BER's (below $10^{-5}$ or so), the upper and lower bounds tend toward each other, while the simulated BER lies between them.[2]

Fig. 3 shows the optical average-power (and electrical SNR) required for 4-PPM to achieve $10^{-6}$ BER on a collection of multipath channels at bit rates of both 10 and 30 Mb/s, as a function of the channel rms delay spread divided by the bit duration.[3] At low delay spreads, equalization provides little, if any, performance improvement. As the delay spread increases, the DFE's provide a significant performance improvement, leading to a finite power requirement for all channels, even those having an infinite power requirement without equalization. Since the symbol-rate ZF-DFE utilizes the information contained in the noncancelled intrasymbol interference, it outperforms the chip-rate ZF-DFE, and performs nearly as well as MLSD on the channels considered here.

## VI. Conclusions

We analyzed both a chip-rate ZF-DFE and a symbol-rate ZF-DFE for PPM systems. Simulations showed that our analysis is accurate at low BER's. We applied our analytical results to a variety of experimentally measured indoor infrared channels, and found that the ZF-DFE performance is very close to MLSD on the channels considered.

## References

[1] F. R. Gfeller and U. H. Bapst, "Wireless in-house data communication via diffuse infrared radiation," *Proc. IEEE*, vol. 67, pp. 1474–1486, Nov. 1979.
[2] M. D. Kotzin, "Short-range communications using diffusely scattered infrared radiation," Ph.D. dissertation, Northwestern Univ., June 1981.
[3] J. R. Barry, *Wireless Infrared Communication*. Boston, MA: Kluwer Academic, 1994.
[4] J. M. Kahn and J. R. Barry, "Wireless infrared communications," *Proc. IEEE*, vol. 85, pp. 265–298, Feb. 1997.
[5] J. M. Kahn, W. J. Krause, and J. B. Carruthers, "Experimental characterization of nondirected indoor infrared channels," *IEEE Trans. Commun.*, vol. 43, pp. 1613–1623, Feb./Mar./Apr. 1995.
[6] G. W. Marsh and J. M. Kahn, "Performance evaluation of experimental 50-Mb/s diffuse infrared wireless link using on-off keying with decision-feedback equalization," *IEEE Trans. Commun.*, vol. 44, pp. 1496–1504, Nov. 1996.
[7] M. R. Pakravan and M. Kavehrad, "Direction diversity for indoor infrared wireless communication receivers," in *Proc. IEEE Int. Conf. Communications*, Seattle, WA, June 19–21, 1995, pp. 1163–1167.
[8] M. D. Audeh, J. M. Kahn, and J. R. Barry, "Performance of pulse-position modulation on measured nondirected indoor infrared channels," *IEEE Trans. Commun.*, vol. 44, pp. 654–659, June 1996.
[9] G. Prati and R. M. Gagliardi, "Decoding with stretched pulses in laster PPM communications," *IEEE Trans. Commun.*, vol. 31, pp. 1037–1045, Sept. 1983.
[10] J. R. Barry, "Sequence detection and equalization for pulse-position modulation," in *Proc. IEEE Int. Conf. Commun.*, New Orleans, LA, May 2–4, 1994, pp. 1561–1565.
[11] J. G. Proakis, *Digital Communications*, 2nd ed. New York: McGraw-Hill, 1989.
[12] G. D. Forney, "Maximum-likelihood sequence estimation of digital sequences in the presence of intersymbol interference," *IEEE Trans. Inform. Theory*, vol. 18, pp. 363–378, May 1972.
[13] J. Salz, "Optimum mean-square decision feedback equalization," *Bell Syst. Tech. J.*, vol. 52, pp. 1341–1373, Oct. 1973.

[2] It is worth noting that for both DFE's, error propagation was not observed at BER's below $10^{-4}$.

[3] The optical power requirement is normalized to the requirement for OOK (or 2-PPM) on a memoryless channel.